Proceedings of the 11th International Conference on Fluid Flow, Heat and Mass Transfer (FFHMT 2024)
Chestnut Conference Centre - University of Toronto, Toronto, Canada – June 16-18, 2024
Paper No. 025
DOI: 10.11159/ffhmt24.025

Induced Flow Field by an Array of Four Synthetic Jet Actuators Issued in a Quiescent Surrounding

Hossein Khanjari[1], Ronald Hanson[1]
[1]Department of Mechanical Engineering, Lassonde Research Centre, York University
4751 Keele St, Toronto, Canada
khanjari@yorku.ca; hansonre@yorku.ca

Abstract **–** The induced flow by an array of four synthetic jet actuators with rectangular orifices with a fixed aspect ratio and a fixed centre-to-centre spacing of 8 mm between the jets, at a constant Reynold number (*Re*) of 660, and three frequencies, that define the Strouhal number (*St*), is studied experimentally. Five phase differences ($\Delta\phi$) from 0° to 180° are applied between the actuators on the far right and the far left and the two middle ones. It is shown that the induced flow field is strongly influenced by the Strouhal number, and phase difference between the actuators. Phase differences of $\Delta\phi = 45°$, and 90° show constructive interaction between the induced flows by the array of actuators. For the higher Strouhal numbers the results indicate less decay in the time averaged velocity.

Keywords**:** Flow Control, Jets, Vortex Interaction

1. Introduction

Synthetic jet actuators (SJAs) are active flow control actuators generally comprising an enclosed cavity with an orifice through which the air flows to the cavity and an oscillating diaphragm (Glezer, 2002; Berk T. a., 2016). The oscillatory motion of the diaphragm generates pressure fluctuation at the edge of the orifice due to the cavity's volume variation (Glezer, 2002; Berk T. a., 2016). The expansion of the volume causes a low internal pressure and air to be ingested to the cavity. The pressure increases as the cavity's volume shrinks, causing the ingested air to be expelled into the surroundings. These two cycles are called ingestion and expulsion cycles, respectively (Glezer, 2002). The periodic occurrence of the expulsion cycle generates train of vortex rings, formed when the air flow leaves the orifice's edge and travels away under their self-induced velocity (Glezer, 2002). The oscillation frequency and the amplitude of a SJA should follow the formation criterion to form a coherent vortex ring otherwise the generated vortex during the expulsion cycle is ingested back to the cavity due to the following suction cycle (Holman, 2005). For circular orifices, the advection of the vortices to the downstream decays causes the interaction of the consecutive vortices and breakdown to smaller structures and ultimately transition to fully turbulent flow (Xia, 2018). For non-circular orifices axis-switching of the vortices causes higher decay rates (Straccia, 2021).

The following parameters are commonly used to characterize the output and geometry of a SJA with a rectangular orifice (Glezer, 2002):

$$\bar{\bar{U}} = \frac{1}{T}\int_0^{T/2} u_t . \mathrm{d}t \tag{1}$$

$$Re = \frac{\bar{U}d}{\upsilon} \tag{2}$$

$$St = \frac{fd}{\bar{U}} \tag{3}$$

$$AR = \frac{l}{d} \tag{4}$$

In Eq. (1), $\overline{U}$ is referred to as mean blowing velocity and usually is calculated during the expulsion cycle. T is the period of the signal in seconds, u_t is the instantaneous jet centreline velocity. Reynolds number (Re) can be calculated using Eq. (2) in which d is the characteristic length of the orifice, that in this study is the width of the orifice; and υ is the kinematic viscosity. The Strouhal number can be given by Eq. (3). In this equation $f = 1/T$, is the actuator's operating frequency. The aspect ratio (AR) of the orifice exit can be given by Eq. (4), where l is the length of the orifice.

The interaction of the vortices generated by SJAs with a crossflow has been the subject of much research as it has a wide range of applications, including flow control. The interaction of the induced flow structures by a SJA into a crossflow creates a blockage that causes momentum transfer between the crossflow and the structures (Berk T. a., 2019). Due to this momentum transfer the induced structures by the SJA are tilted to the flow direction while accelerating until they reach the flow velocity (Berk T. a., 2019). The resulting structures' shape and their downstream development depends on a variety of parameters, including the orifice geometry and orientation with respect to the freestream, Strouhal number, and blowing ratio (Berk T. a., 2019; Van Buren, 2016; Belanger, 2020). For a SJA, the blowing ratio can be given by $r = \overline{U}/U_\infty$, where U_∞ is the freestream velocity. In a boundary layer, a SJA can be used to induce streamwise vortices. This type of vortical structure can be used to suppress existing structures in boundary layers via a flow control strategy known as "Opposition Control" (Kim, 2011; Rathnasingham, 2003). For example, Rathnasingham *et al.* (Rathnasingham, 2003) used SJAs with rectangular orifices, that its orifice is elongated parallel to the flow direction, to manipulate the near-wall bursting events in a turbulent boundary layer and reported a 7% reduction in the wall shear stress.

It is believed that a realistic approach for controlling the streamwise elongated structures in a boundary layer necessitates the use of arrays over single isolated actuators [11, 12]. Arrays of actuators imposes two additional parameters that would affect the resulting induced flow, the spacing between the actuators (Δ) and their relative operating phase ($\Delta\phi$). Berk *et al.* (Berk T. a., 2016) studied the vectoring of the issued jets by two SJAs with rectangular orifice in a quiescent flow. They showed that different vectoring angles can be achieved, which is primarily dependent on the St, Δ, and $\Delta\phi$ (Berk T. a., 2016). In addition, they have shown the negligible effect of the Re on the vectoring angle. In a later study by Jankee *et al.* (Jankee, 2021), an array of two SJAs were placed in a turbulent boundary layer to consider the effect of the Δ, and $\Delta\phi$. It is shown that if the actuators are close enough, the crossflow only causes a temporal and spatial delay on the interaction of the jets and therefore the resulting vectoring behaviour (Jankee, 2021). There is a very limited body of literatures on the arrays of more than two SJAs. Pasa *et al.* (Pasa, Influence of Strouhal number and phase difference on the flow behavior of a synthetic jet array, 2022) studied an array of four SJAs numerically. They considered the effect of the St, and $\Delta\phi$, and showed that for some Strouhal numbers the resulting induced flow remains invariant for phase angle variation (Pasa, Influence of Strouhal number and phase difference on the flow behavior of a synthetic jet array, 2022). For a Strouhal number, $St = 0.086$, the phase angle variation has an influence and maximum vectoring angle can be achieved when actuators have 90° phase difference. Pasa *et al.* (Pasa, Focusing of jet from synthetic jet array using non-linear phase delay, 2023) used the vectoring concept to focus the induced flow by an array of four SJAs. The two middle SJAs were the leading actuators while the two outer actuators in the array lagged in phase. The two middle actuators, however, had the same operating phase (Pasa, Focusing of jet from synthetic jet array using non-linear phase delay, 2023). Their studies showed that an increase of 52% fort the time averaged streamwise velocity is achievable for the case of $St = 0.086$, and $\Delta\phi = 90°$ (Pasa, Focusing of jet from synthetic jet array using non-linear phase delay, 2023). Choice of operating parameters for arrays of SJAs can have a significant effect on the result flow and therefore would influence actuator design and operation for flow control applications.

In the present study, the flow output of an array of four SJAs is examined experimentally. The output of the array of the SJAs is measured using constant temperature anemometry (CTA). The structure of this paper is as follows. Section 2 provides the details of the experiment, including the design of the actuators, the measurement method and calibration of the jets. Section 3 discusses the results in terms of the mean flow, followed by concluding remarks in Section 4.

2. Experimental Set-up and Methodologies

The array consists of four SJAs with rectangular offices that are placed side-by-side as shown in Fig. 1. The actuators are driven by four Visaton FRS 8 M speakers, which are used to generate the oscillatory motion required for a SJA. The speakers have a frequency response of 100 to 20000 Hz, with an impedance of 8 Ω and a rated power of 30 W, which limits the maximum applied voltage (V_{pp}) to 15.5 V. The resonant frequency of the speakers occurs near 120Hz. The four speakers are excited by two Sound Town Professional amplifiers, each with two channels. The initial driving sine wave is created

using two Rigol dg1022 function generators (FGs). The setup results in four channels, one for each speaker, to account for differences in the individual SJA calibrations.

The actuator body containing the cavity is printed using a PLA printer with 0.15 mm filament and 100% infill. The resulting cavity has a volume of 1.22×10^{-5} m^3, excluding the volume of the speaker. Figure 1a shows a schematic of the array of the actuators. As shown in this figure, the body of the cavities has a total thickness of 8 mm, which is the limiting factor in the spacing between the actuators. Although this limiting factor can be overcome with a higher resolution printer, it would cost nearly 15 times more expensive printing. As shown in Fig. 1a the cavities are mounted to a machined aluminium plate which allows maximum spacing of 40 mm between jets. Prior to mounting the cavities, the orifices that are all printed as one part, and herein referred to as orifice plate, will be located in their place as shown in Fig. 1a. Figure 1b provides a closer view to the orifice plate. The orifice plate is printed using a high-resolution multijet printer with an accuracy of 0.05 mm. The orifice exit has a 13 mm length and 1 mm width, resulting in an aspect ratio of $AR = 13$ (see Fig. 1b). The aspect ratio in this research is kept constant. The length of the orifices' neck is 10 mm.

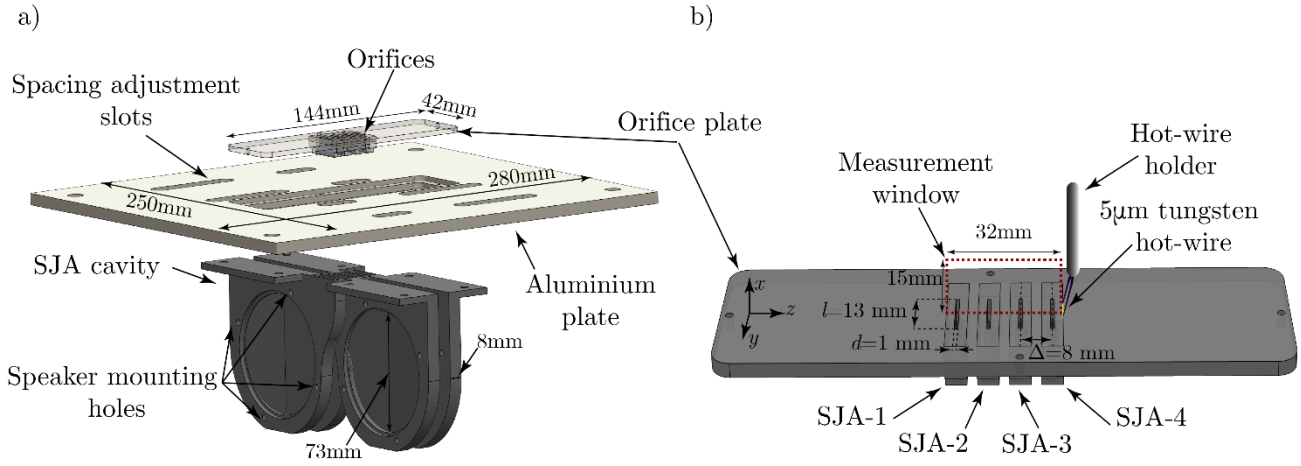

Figure 1: a) Schematic of the array of four actuators, showing the cavities, the orifice plate and the plate that holds the actuators, b) closer view of the orifice plate, the orifice exits and the hot-wire probe.

The output of the actuators is measured using constant temperature anemometry (CTA). In this regard, a Hanghua CTA-04 anemometry system with a 5μm single wire probe that has an overheat ratio of 1.8 is used. The hotwire is mounted to a 3D traverse system to measure the outputs of the jets. The hot-wire is calibrated before and after each experiment, to account for the temperature drifts. The uncertainty of less than 2% is achieved for the hot-wire calibration. The measurement region considered is shown in Fig. 1b and has width (z) of 32 mm and height (x) of 15 mm, with resolution of 0.25 mm and 1 mm in z and x directions respectively. The measurement region starts from 1 mm off the wall. The output of each of the actuators is calibrated for all operating conditions prior to the spatial measurement, with the probe located at the centre of the orifice exit, to apply enough input to the actuators to achieve similar mean blowing velocity. It is worth mentioning that although the CTA measurement is limited to only the velocity magnitude, it helps picturing the induced flow by the array of actuators, as shown in this research.

The output of the actuators are calibrated for applied voltages of V_{pp} = 4, 5.5, 7, 8.5, 10, 12, and 14 V, and frequencies from $f = 300$ Hz to 800 Hz, with the increment of 20 Hz. One amplifier channel was used for the calibration of all actuators to ensure the exact similar output and applied voltage. The hotwire probe was placed at the centre of the actuators, and x = 0. The CTA measurement for calibrating the actuators had sampling rate of 42 KHz for the duration of 5 seconds. The resulting signals are phase averaged against the signal from function generator. The mean blowing velocity is calculated during the expulsion cycle of the phase averaged signal. The resulting output of the jets are shown for the actuators in Fig. 2a. Although the resulting flow output is different for the SJAs at the same operating condition, the overall behaviour of their

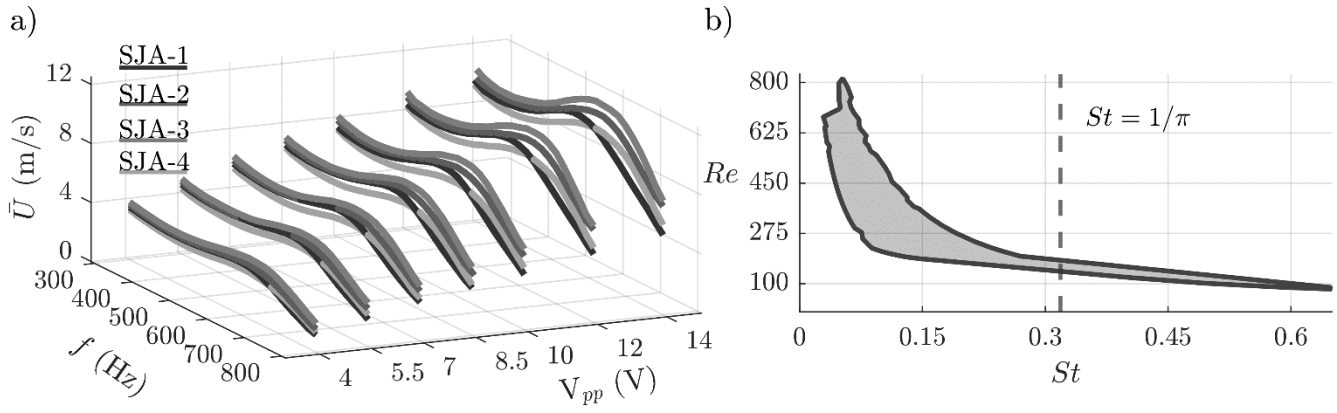

Figure 2. a) Output of the actuators in the present study at various operating conditions in terms of mean blowing velocity, operating frequency and applied voltage, b) output of the actuators during the calibration in terms of Strouhal and Reynolds number. The dashed line indicates the formation criterion.

output is similar. As shown in Fig. 2a, increasing the amplitude of the driving signal leads to increase in the output of the jets. Furthermore, as illustrated, the increasing the frequency from 300 Hz to near 450 Hz shows a decay in the jets' output, because of the deviation from the resonant frequency of the speakers. The output of the SJAs start to increase and peaks near 600 Hz, which is the Helmholtz resonant frequency (f_h). For a SJA one of the maximum outputs occurs at the Helmholtz resonant frequency (f_h), and SJAs have their highest energy efficiency at this frequency (Gil, 2021). The f_h is given as follows:

$$f_h = \frac{c}{2\pi}\sqrt{\frac{A}{\bar{U}.L}} \tag{5}$$

where c is the speed of the sound, A is the orifice surface area, and L is the orifice neck length. Based on the actuator's characteristics, that are discussed earlier the resulting theoretical f_h= 565 Hz, which is close to the results from the experiments. Figure 2b shows the range of the St, and Re numbers at which the actuators are calibrated. As shown in this figure, above the formation criterion ($St = 1/\pi$), shown by a dashed line, the actuators have low output. However, the range of the considered Strouhal numbers is well before the formation criterion that ensures the formation and advection of the train of vortices.

3. Results and Discussion

The output of the actuators for a constant Reynolds number of 660, with varying Strouhal numbers, is studied over the region of the measurement window. The frequency varies between 300 Hz and 600 Hz, with 150 Hz spacing, corresponding to Strouhal numbers of 0.03, 0.045, and 0.06, respectively. The two middle actuators are set to be the leading actuators, while the two extreme actuators are triggered with a phase difference ($\Delta\phi$) of 0° to 180°, with respect to the leading actuators. Figure 3 a to e illustrates time-averaged velocity (V_{avg}), for $\Delta\phi = 0°$ to 180°, respectively for increments of 45°. In this figure, the location of the actuators is shown by blue areas at z/d = -12, -4, 4, and 12 just above the actuator outlets. It is visually evident that the variation of St, and $\Delta\phi$, leads to changes in the induced flow field. For all relative phase angles, the increase in the Strouhal number has led to higher velocity contour levels at $x/d > 5$. In addition, the induced flows by different actuators will interact as they advect away from the orifice edge while they are independent of each other close to the orifice exits. The interaction between the induced flow for each Strouhal number is shown to change with the relative phase angle. The time-averaged velocity across the span at three different streamwise regions of near-field ($x/d = 1$), intermediate-field ($x/d = 7$), and far-field region ($x/d = 12$), are shown in Fig. 4. The three streamwise location are shown with dashed line in Fig. 3e at $St = 0.03$. Figure 4 a to e corresponds to the relative phase angles of 0° to 180°. The location

from the wall in terms of *x/d* of each column of these plots is shown above the column. For $x/d = 1$, the time-averaged velocity along *z/d* are similar for all operating conditions suggesting that the variation of the Strouhal number and $\Delta\phi$, has no impact on the induced flow in this region. The spanwise variation (along *z/d*) of the time-averaged velocities shows peaks right above the exit of the orifices, which are generated by the flow output by the actuators at this height. These jets appear to be isolated at this location, however, the merging jets are more apparent at larger values of *x/d*.

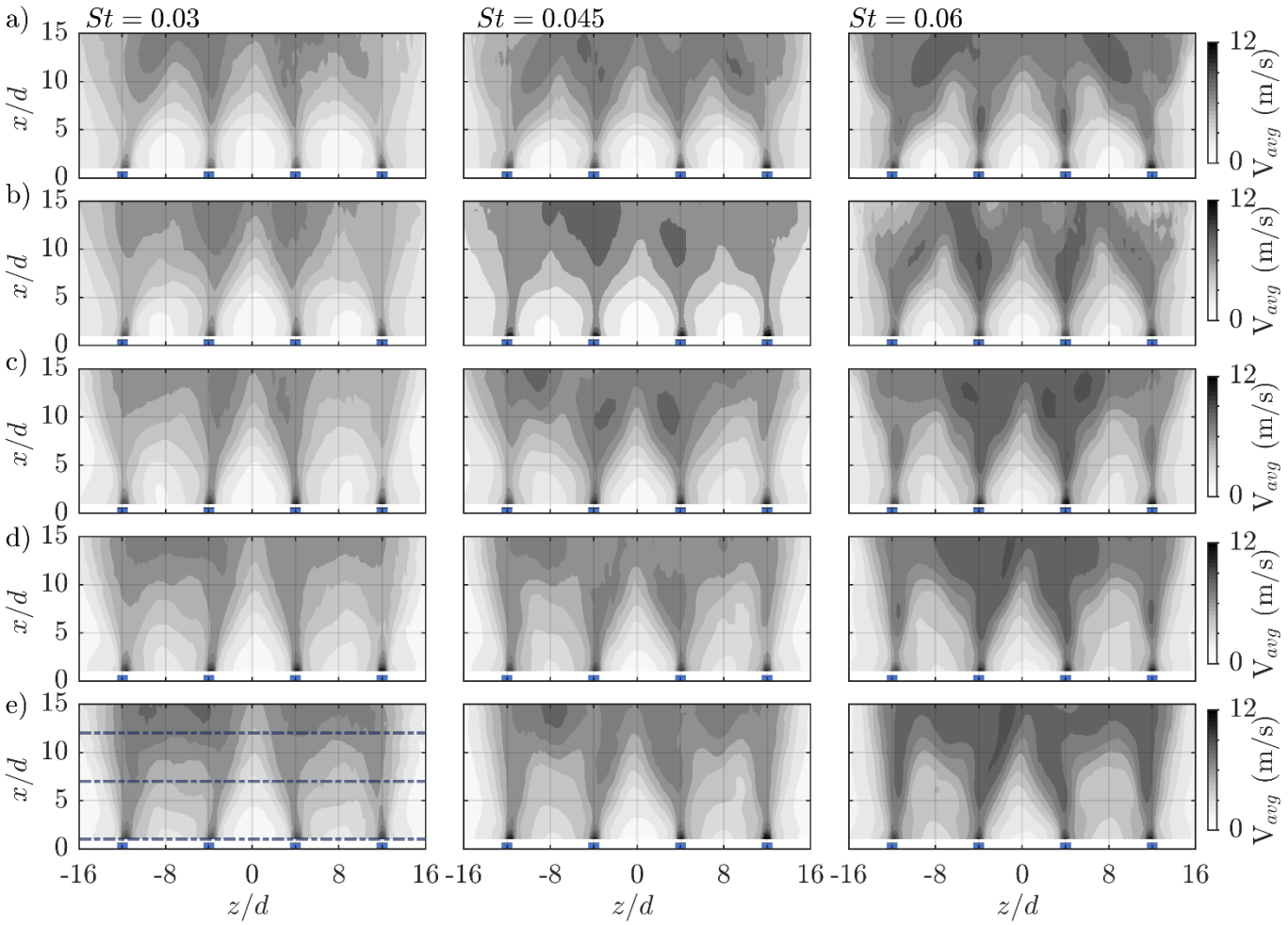

Figure 3. Time averaged velocity above the array of SJAs for St = 0.03, 0.045, and 0.06, at $\Delta\phi = 0°\ to\ 180°$ from the start of the expulsion cycle of actuators 2, and 3, shown in rows a to e.

At the intermediate region where *x/d* = 7, the merging velocity profiles suggest a decay in the time average velocity compared to the near-field region (*x/d* = 1), which decreases with an increase in the Strouhal number. At this streamwise region, at all relative phase angles, the region in between the actuators shows an increase in velocity, which implies that the induced vortices have accelerated the flow in these regions while they remain coherent, as evident from their well-defined peaks in the velocity profiles across the span. For $\Delta\phi = 0°$, the flow occurring between the middle actuators and the two extreme actuators shows a significant increase close to the outer actuators. This can be an indication that the spatial development of the induced vortices between the outer actuators and the middle actuators has been a constructive interaction as it has led to a higher velocity level compared to the flow between the middle actuators. The entrainment of the flow by SJA 1 and 4 to the ambient flow can be responsible for this flow response which could have resulted in rearranging the flow such that it has led to a constructive interaction between the vortices. As $\Delta\phi$ has increased this flow behaviour between the middle actuators and their neighbouring outer actuators become less evident. For $\Delta\phi = 45°$ and 90°, the peaks above the two middle actuators show higher values compared to the two peaks above the two extreme actuators, which can be an

indication of constructive interaction of the flows toward the middle of the actuators. At $\Delta\phi = 135°$ and 180°, the difference between the peaks is decreased.

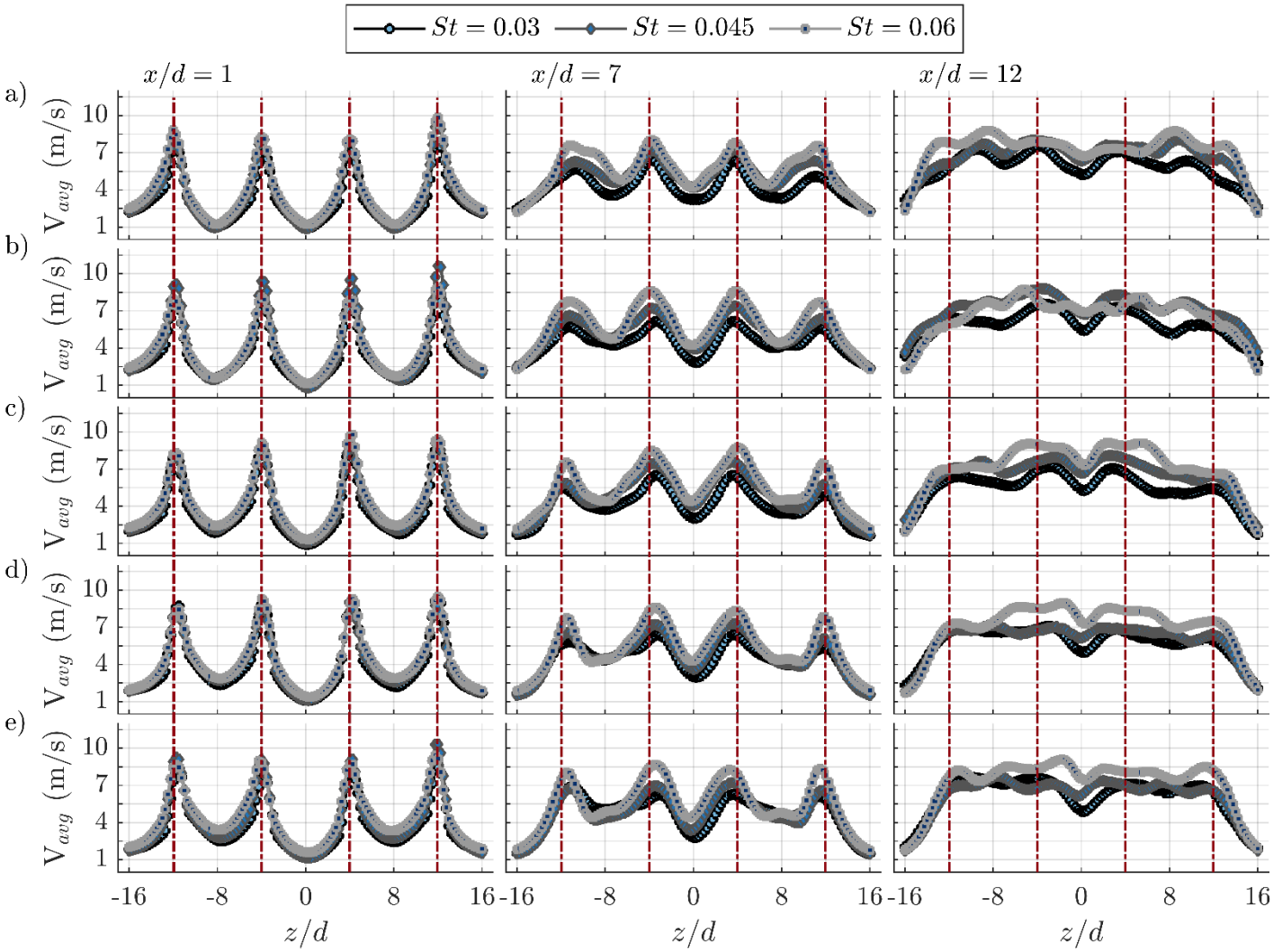

Figure 4 The spanwise variation of the time-averaged velocity at three different streamwise locations for three different Strouhal numbers for the array of actuators. In this figure, rows a to e correspond to $\Delta\phi = 0°$ to $\Delta\phi = 180°$. The red dshed-dotted lines indicate the location of the SJAs' outlet.

At the far-field region ($x/d = 12$), the flow output of the jets the interaction and breakdown of the jets has become evident as the previous four well-define peaks corresponding to the four jets do not remain. Although the regions close to the edge of the measurement window in the span are accelerated, the induced flow by the array of the actuators has not spread into the span beyond the $z/d < -16$, and $z/d > 16$, which is evident by the low velocity magnitude at the edge of the measurement window. At $\Delta\phi = 0°$, for all Strouhal numbers the decay in the velocity is very similar. However, at higher $\Delta\phi$, the flow appears to be focused around the middle of the measurement window. In addition, the decay of the velocity shows to be more for lower Strouhal numbers compared to the maximum case.

4. Conclusion

In this study, the induced flow above an array of 4 synthetic jet actuators under various operating conditions is studied experimentally using constant temperature anemometry. The time-averaged velocity contour maps and plots for the time-averaged velocity along the span suggest the dependency of the induced flow field on both the Strouhal number and the relative phase angles between the operation of the actuators. For the two relative phase angles of $\Delta\phi$ equals 45 degrees , 90 degrees , the interaction of the induced structures by the array of actuators is more constructive compared to the other $\Delta\phi$ as they have led to a higher time-averaged velocities above the two middle actuators. In addition, the increase in the Strouhal number shows lower decays in almost all cases.

5. References

[1] A. Glezer, M. Amitay, "Synthetic jets," *Annual review of fluid mechanics,* vol. 34, pp. 503-529, 2002.

[2] T. Berk, G. Gomit, and B. Ganapathisubramani, "Vectoring of parallel synthetic jets: a parametric study," *Journal of Fluid Mechanics,* vol. 804, pp. 467-489, 2016.

[3] R. Holman, Y. Utturkar, R. Mittal, B. L. Smith, and L. Cattafesta, "Formation criterion for synthetic jets," *AIAA journal*, vol. 43, pp. 2110-2116, 2005.

[4] X. Xia, and K. Mohseni, "Transitional region of a round synthetic jet," Physical Review Fluids, vol. 3, p. 011901, 2018.

[5] J. C. Straccia, and J. AN. Farnsworth, "Axis switching in low to moderate aspect ratio rectangular orifice synthetic jets," Physical Review Fluids, vol. 6, p. 054702, 2021.

[6] T. Berk, and B. Ganapathisubramani, "Effects of vortex-induced velocity on the development of a synthetic jet issuing into a turbulent boundary layer," Journal of Fluid Mechanics, vol. 870, pp. 651-679, 2019.

[7] T. Van Buren, and C. M. Leong, and E. Whalen, and M. Amitay, "Impact of orifice orientation on a finite-span synthetic jet interaction with a crossflow," Physics of Fluids, vol. 28, 2016.

[8] R. Belanger, D. Zingg, P. Lavoie, "Vortex structure of a synthetic jet issuing into a turbulent boundary layer from a finite-span rectangular orifice," AIAA Scitech, 2020.

[9] J. Kim, "Physics and control of wall turbulence for drag reduction," Philosophical Transactions of the Royal Society A: Mathematical, Physical and Engineering Sciences, vol. 369, pp. 1396-1411, 2011

[10] R. Rathnasingham, and K. S. Breuer, "Active control of turbulent boundary layers," *Journal of Fluid Mechanics,* vol. 495, pp. 209-233, 2003.

[11] G. K. Jankee, and B. Ganapathisubramani, "Interaction and vectoring of parallel rectangular twin jets in a turbulent boundary layer," *Physical Review Fluids,* vol. 6, p. 044701, 2021.

[12] J. Pasa, and S. Panda, and V. Arumuru, "Influence of Strouhal number and phase difference on the flow behavior of a synthetic jet array," *Physics of Fluids*, vol. 34, 2022.

[13] J. Pasa, and S. Panda, and V. Arumuru, "Focusing of jet from synthetic jet array using non-linear phase delay," *Physics of Fluids*, vol. 35, 2023.